Thermal stability and oxidation of layer-structured rhombohedral In3Se4 nanostructures

Guang Han, Zhi-Gang Chen, Lei Yang, Lina Cheng, Kevin Jack, John Drennan, and Jin Zou

Citation: Applied Physics Letters **103**, 263105 (2013); doi: 10.1063/1.4857655
View online: http://dx.doi.org/10.1063/1.4857655
View Table of Contents: http://scitation.aip.org/content/aip/journal/apl/103/26?ver=pdfcov
Published by the AIP Publishing

Thermal stability and oxidation of layer-structured rhombohedral In_3Se_4 nanostructures

Guang Han,[1] Zhi-Gang Chen,[1,a)] Lei Yang,[1] Lina Cheng,[1] Kevin Jack,[2] John Drennan,[2] and Jin Zou[1,2,a)]
[1]*Materials Engineering, The University of Queensland, Brisbane QLD 4072, Australia*
[2]*Centre for Microscopy and Microanalysis, The University of Queensland, Brisbane QLD 4072, Australia*

(Received 26 November 2013; accepted 11 December 2013; published online 26 December 2013)

The thermal stability and oxidation of layer-structured rhombohedral In_3Se_4 nanostructures have been investigated. *In-situ* synchrotron X-ray diffraction in a sealed system reveals that In_3Se_4 has good thermal stability up to 900 °C. In contrast, In_3Se_4 has lower thermal stability up to 550 or 200 °C when heated in an atmosphere flushed with Ar or in air, respectively. The degradation mechanism was determined to be the oxidation of In_3Se_4 by O_2 in the heating environment. This research demonstrates how thermal processing conditions can influence the thermal stability of In_3Se_4, suggesting that appropriate heating environment for preserving its structural integrity is required. © *2013 AIP Publishing LLC*. [http://dx.doi.org/10.1063/1.4857655]

The thermal stability is a measure of the resistance of a material to transformation and/or decomposition at elevated temperatures and is an important intrinsic characteristics of any material.[1] For example, for a given material, having a superior thermal stability is important for high-temperature applications, such as thermoelectric energy conversion,[2–4] high-temperature catalytic reactions,[5] and for use in fuel cells.[6] Therefore, extensive investigations have been performed to explore the material thermal stability in bulk or nanoscale forms.[7–12] The thermal stability of a material is not only determined by the intrinsic crystal structure but is also influenced by the conditions under which the heating is performed, such as the heating environment.[3] Oxidation, revealing the instability of materials under O_2 environment, always reduces the material thermal stability and results in the degradation of their intrinsic property.[13] On the other hand, oxidation can also be used to tune the photoelectric property of materials[14] and to intentionally design metal oxides with specific morphology.[15–23] Understanding the oxidation behaviour can then extend the routes in preserving materials' structural integrity under elevated temperatures.

Layer-structured indium selenides have attracted much attention in high-temperature thermoelectric applications due to their excellent electrical and thermal properties.[24–28] In particular, it has been shown that nanostructured indium selenides have the potential to provide better thermoelectric properties than their bulk counterparts, due to the enhanced phonon scattering by increased interfaces and boundaries.[27] Many investigations have been carried out to understand the thermal stability and oxidation behaviour of various bulk indium selenides.[15,16,20,21,29–34] In contrast, however, there are very limited investigations on the thermal stability and oxidation of indium selenide nanostructures. For example, κ-In_2Se_3 nanowires were revealed to be stable up to 500 °C by *in-situ* synchrotron X-ray diffraction (XRD).[35] In thin layers of α-In_2Se_3, an increased temperature of the $\alpha \rightarrow \beta$ transition was observed as the layer thickness decreases, indicating that the α phase has enhanced thermal stability in the thin-layer form.[36] However, to date, there are no reported systematic investigations of the thermal stability (including the oxidative stability) of other indium selenide nanostructures, including a new nanostructured In_3Se_4 phase, which was very recently reported by this group.[37] To better understand the potential high-temperature applications of this indium selenide phase, it is necessary to investigate the structural and morphological characteristics of In_3Se_4 nanostructures under different heating conditions.

In this study, we used *in-situ* synchrotron XRD measurements to study the thermal stability (up to 900 °C) of In_3Se_4 powders, which were sealed in a capillary and hence isolated from ambient O_2. Additionally, the influence of the atmospheres under which the heating was carried out on the thermal stability of In_3Se_4 was also investigated by carrying out *ex-situ* XRD measurements on samples, which were subjected to heating in an unsealed environment and while being flushed with Ar or in air. The measurements provide both the temperature at which degradation occurs as well as providing details of the products of degradation.

In_3Se_4 nanostructures were synthesized using an ethylenediaminetetraacetic acid assisted solvothermal method.[38] To study the thermal stability of In_3Se_4, *in-situ* synchrotron XRD measurements of the In_3Se_4 during heating were performed on the powder diffraction beamline at Australian Synchrotron. For this particular analysis, In_3Se_4 powders were loaded into a quartz capillary and sealed at both ends, in order to entirely isolate the investigated sample from ambient O_2. The capillary was progressively heated from room temperature (RT) to 300, 500, 700, and 900 °C, at a rate of 5° per min, and the diffraction patterns were obtained at each temperature over a period of 20 min (2 × 10 min acquisitions). All of the XRD measurements were collected in transmission geometry using a Mythen detector and at a wavelength of 1.0000 Å (determined through the refinement of a LaB_6 standard).

To investigate the thermal stability and oxidation of In_3Se_4 under different environments, In_3Se_4 powders were

a)Electronic addresses: j.zou@uq.edu.au and z.chen1@uq.edu.au

loaded into a tube furnace and annealed to various temperatures under different environments, namely, 550, 650, and 900 °C for Ar and 200, 300, and 400 °C for air, respectively. As the heating system is not completely sealed, a small amount of air inclusion is expected even when the heating atmosphere is flushed with Ar, although the concentration of O_2 will be significantly reduced compared with heating in pure air. The sample was held at each annealed temperature for 2 h to stabilize the structures after annealing. The crystal structures of the annealed samples were determined by XRD measurements, which were obtained on a Bruker MKIII D8 Advance X-ray diffractometer in Bragg-Brentano geometry. The system is equipped with a sealed tube Cu K_α radiation (X-ray wavelength: 1.5408 Å) source and a Lynxeye multi-strip detector. The morphologies of the samples were investigated by scanning electron microscopy (SEM, JEOL 7800 operated at 5 kV), and their crystallographic characteristics were analyzed by transmission electron microscopy [TEM, Philips FEI Tecnai F20, operated at 200 kV and equipped with the energy-dispersive spectroscopy (EDS) for compositional analysis].

Figure 1(a) shows a series of *in-situ* synchrotron XRD patterns of the synthesized products before, during, and after the annealing process within a temperature range from RT to 900 °C. Figure 1(a-i) is the XRD pattern of the as-synthesized product at RT, in which all of the diffraction peaks can be indexed to the layer-structured rhombohedral In_3Se_4.[38] Figures 1(a-ii)–1(a-v) show the XRD patterns of the synthesized product annealed at 300, 500, 700, and 900 °C in a sealed capillary, respectively, and Figure 1(a-vi) is the XRD pattern of sample at RT following annealing to 900 °C. It can be seen from all of these patterns that there are no changes to the crystal structure of the sample during this heating cycle and this indicates the stability up to 900 °C of crystalline nature of the synthesized In_3Se_4 when heated in the sealed system. This stability of In_3Se_4 is in strong contrast to those of currently available layer-structured indium selenides, such as In_4Se_3 (melting point at ~550 °C),[39] γ-InSe (melting point at ~600 °C),[39] and α-In_2Se_3 (transformation to β-In_2Se_3 at ~200 °C).[39] It should be noted that the peaks of (102) (at ~17°) and (113) (at ~29.5°) gradually disappeared during the heating process, which could be due to the increase of grain size or preferential orientation induced by heating. Figures 1(b)–1(d) show the morphological and nano-scale structural characteristics of the synthesized In_3Se_4 nanostructures by electron microscopy. As can be seen, the as-synthesized nanostructures have a flowerlike morphology with an overall diameter of 3–9 μm, which is assembled from ~20 nm nanosheets. Figures 1(e)–1(g) present the electron microscopy investigations of the products at RT after being annealed at 900 °C, and it can be seen that the morphology of the In_3Se_4 is not significantly changed, i.e., the nanosheet-assembled flowerlike nanostructures are observed. In combination with the XRD results above, it can be seen, therefore, that both the crystalline and nano-scale structures of the In_3Se_4 are stable to heating at up to 900 °C when heated in a sealed environment.

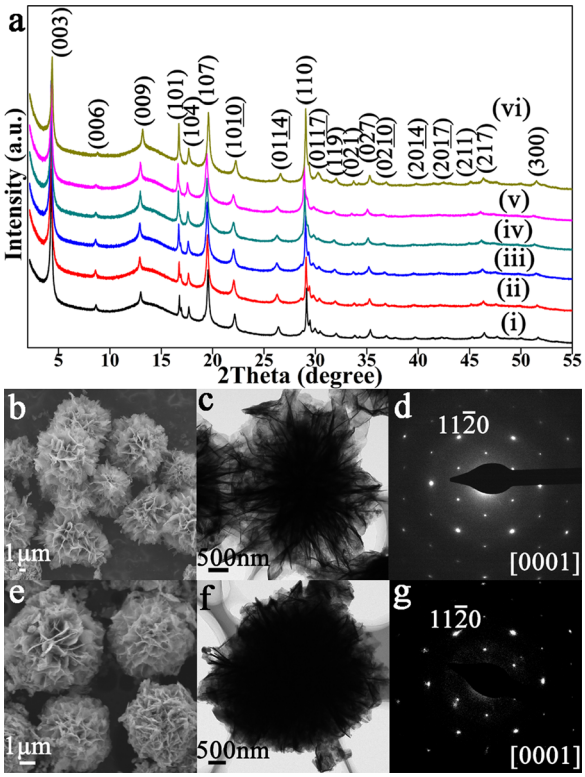

FIG. 1. (a) *In-situ* synchrotron XRD patterns of In_3Se_4 annealed at various temperatures: (i) RT (as-prepared solvothermal sample), (ii) 300 °C, (iii) 500 °C, (iv) 700 °C, (v) 900 °C, and (vi) RT (after heating), and structural and morphological characterizations of the as-synthesized solvothermal In_3Se_4 (b)–(d) and the products after heating In_3Se_4 nanostructures in a sealed capillary at 900 °C (e)–(g): (b) and (e) SEM images, (c) and (f) TEM images, and (d) and (g) typical SAED patterns from a single nanosheet.

To better understand the thermal stability of these In_3Se_4 nanostructures under different environments, we annealed In_3Se_4 nanostructures in unsealed systems: under a flow of Ar gas to exclude the majority of air and also under air. Figure 2 shows structural and morphological characteristics of the synthesized product annealed for 2 h at different temperatures (25, 550, 650, or 900 °C) under a flow of Ar. Figures 2(a-ii) and 2(b)–2(d) are the experimental data taken from the synthesized nanostructures annealed at 550 °C. By comparison of these characterization results with those from the as-synthesized product [refer to Figs. 1(b)–1(d)], it can be seen that the crystal- and nano-structures are essentially unchanged, and that the In_3Se_4 nanostructures are, therefore, thermally stable at temperature of up to 550 °C when heated under an Ar flow. With a further increase in the annealing temperature to 650 °C, weak diffraction peaks belonging to In_2O_3 (JCPDS file no. 71-2195) can be observed in the XRD pattern, as shown in Fig. 2(a-iii), indicating the commencement of oxidation of In_3Se_4. When the synthesized nanostructures were annealed at 900 °C, as revealed in Fig. 2(a-iv), the majority of the crystalline material was observed to become a mixture of In_2O_3 and γ-In_2Se_3 (JCPDS file no. 89-0658). SEM [Fig. 2(e)] and TEM [Fig. 2(f)] investigations show that the products obtained are composed of predominantly particles with a size of tens to hundreds nm dispersed on nanosheet surfaces. Figure 2(g) is a selected area electron diffraction (SAED) pattern taken along the [41$\bar{5}$] zone axis of In_2O_3, confirming the existence of In_2O_3 particles in the annealed products. These facts suggest that the small amount of air that remains in the system with the Ar flow may lead to the decomposition of In_3Se_4 to form

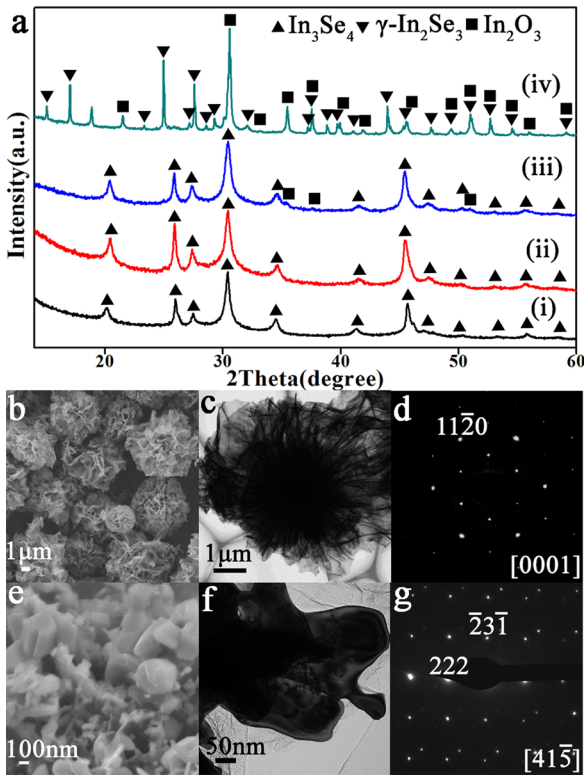

FIG. 2. (a) XRD patterns of the products after annealing In_3Se_4 under an Ar flow: (i) 25 °C, (ii) 550 °C, (iii) 650 °C, and (iv) 900 °C, and structural and morphological characterizations of the products after heating In_3Se_4 nanostructures under Ar flow at 550 °C (b)–(d) and 900 °C (e)–(g): (b) and (e) SEM images, (c) and (f) TEM images, and (d) and (g) typical SAED patterns from a single nanosheet and nanoparticle, respectively.

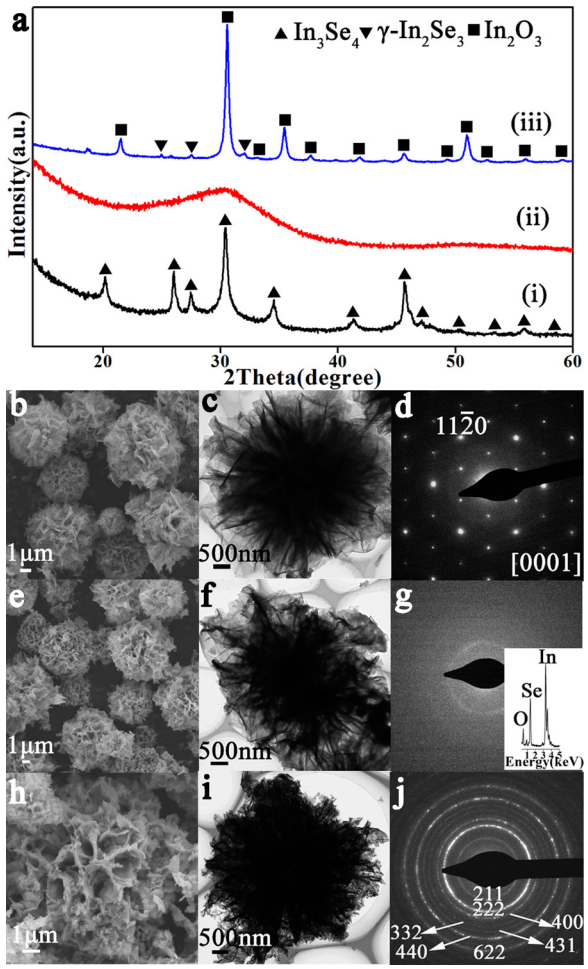

FIG. 3. (a) XRD patterns of the products after heating In_3Se_4 at various temperatures under air: (i) 200 °C, (ii) 300 °C, and (iii) 400 °C, and structural and morphological characterizations of the products after heating In_3Se_4 nanostructures under air atmosphere at (b)–(d) 200 °C, (e)–(g) 300 °C, and (h)–(j) 400 °C: (b), (e), and (h) SEM images, (c), (f), and (i) TEM images, (d), (g), and (j) typical SAED patterns from a single nanosheet. Inset in Fig. 3(g) is the EDS spectrum of the flower in Fig. 3(f).

γ-In_2Se_3 and In_2O_3 at temperatures of above 550 °C. This result suggests that In_3Se_4 is thermally stable up to 550 °C in such a heating environment.

When the synthesized nanostructures are annealed under air (i.e., a much higher O_2 concentration than that in the former two heating environments), different thermal stability and oxidation behaviour can be observed. Figure 3 shows the XRD and electron microscopy characterizations of the In_3Se_4 nanostructures annealed under air at 200, 300, and 400 °C for 2 h. Figures 3(a-i) and 3(b)–3(d) show the structural and morphological characteristics of In_3Se_4 nanostructures annealed at 200 °C, confirming no structural and morphological alternations are observed. Figures 3(a-ii) and 3(e)–3(g) show the experimental investigations of the In_3Se_4 nanostructures that were annealed at 300 °C. It is of interest to note that the products still show a flowerlike morphology, but from the XRD, it can be seen that they are converted into an amorphous structure. EDS analysis [refer to inset in Fig. 3(g)] shows that this sample contains not only In and Se, but also O. These results suggest both that the crystal structure of synthesized nanostructures has been destroyed and that oxidation has been initiated after annealing at 300 °C. With further annealing the nanostructures at 400 °C, a mixture of predominantly In_2O_3 and a small amount of γ-In_2Se_3 can be determined by XRD [refer to Fig. 3(a-iii)], indicating that the significant decomposition of In_3Se_4 has occurred at 400 °C. Figures 3(h)–3(j) show that the products obtained are In_2O_3 flowerlike nanostructures with a polycrystalline structure. From above experimental results, it can be concluded that the higher O_2 concentration in air promotes the oxidation and decomposition of In_3Se_4 and significantly reduce the thermal stability of In_3Se_4. In particular, it can be seen that In_3Se_4 can be oxidized and decomposes more efficiently in air, even when the annealing temperature was only 400 °C.

Based on the above investigation, the thermal stability, oxidation, and decomposition of In_3Se_4 under different annealing environments can be summarized in Fig. 4. It is of interest to note that the layered-structure rhombohedral In_3Se_4 crystals can be retained when annealed at 900 °C in a sealed system isolated from ambient O_2, at 550 °C under Ar flow (which excludes the majority of air), or 200 °C under an ambient air atmosphere, respectively [Fig. 4(a-i)]. In contrast, when annealing was performed at 650 °C under Ar flow or at 300 °C under air atmosphere, incomplete oxidation of In_3Se_4 occurs and results in different products; i.e., In_3Se_4 with a minor amount of In_2O_3 and an amorphous In-Se-O compound, respectively [Fig. 4(a-ii)]. This difference could be due to the different annealing temperature: high temperature could promote the crystallization of In_2O_3, while low temperature can only result in partial replacement of Se with O without significant crystallization of In_2O_3. When annealing was performed at even higher temperature, e.g., 900 °C

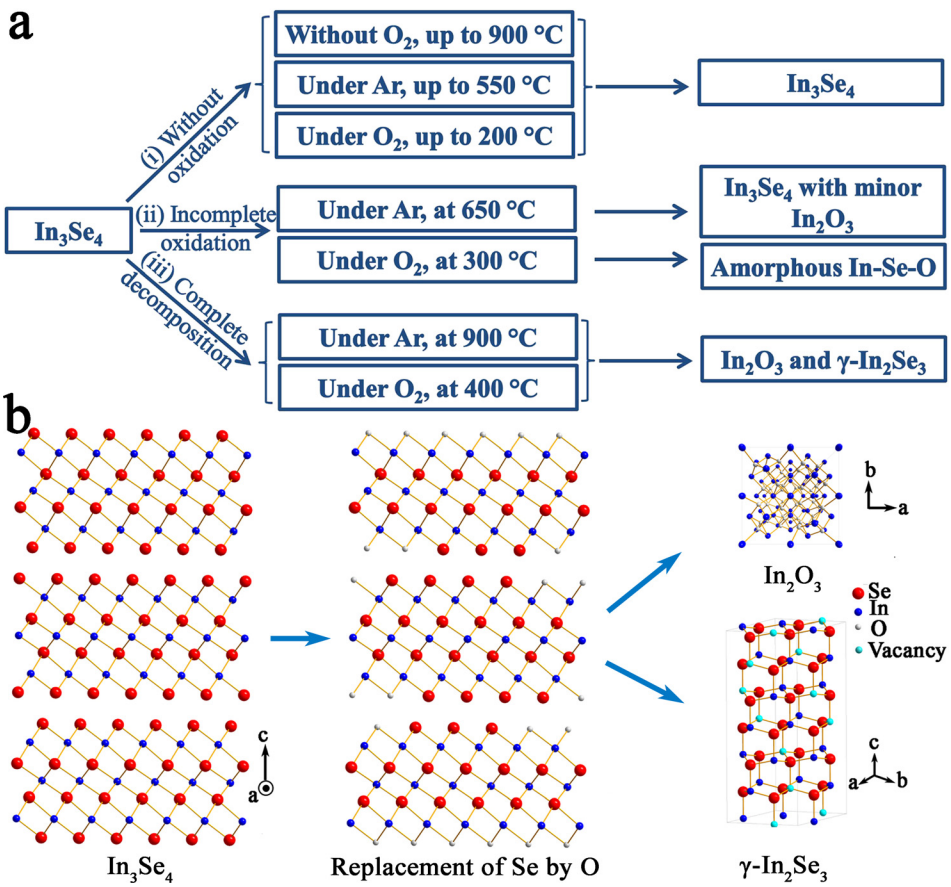

FIG. 4. (a) Summary of thermal stability, oxidation, and decomposition of In_3Se_4 under different annealing environments. (b) Schematic illustration showing the oxidation and complete decomposition of In_3Se_4 [Fig. 4(a-iii)].

under Ar or 400 °C under air, decomposition of the In_3Se_4 and formation of In_2O_3 and γ-In_2Se_3 are enhanced [Fig. 4(a-iii)], as hypothesized in the following steps and as shown schematically in Fig. 4(b). During the annealing process, O is preferentially adsorbed on the nanosheet surface and then replaces Se, which leads to the release of Se atoms from crystal lattice. It should be noted that, with increasing the annealing temperature and/or O_2 concentration, this replacement becomes enhanced.[40] The different atomic radii of O and Se cause a plastically deformed layer, on which the nucleation and following growth of In_2O_3 nanocrystals occur.[15,41] Due to the formation of In_2O_3, the complex layer of Se-In-Se-In-Se-In-Se is broken, resulting in the decomposition of the In_3Se_4 crystal structure. After that, the remaining broken In-Se layers will re-connect with each other to form more stable γ-In_2Se_3. In this study, the remaining amount of γ-In_2Se_3 depends upon the O_2 concentration in the environment and annealing temperature, e.g., very small amount of γ-In_2Se_3 for heating at 400 °C under air, and large amount of γ-In_2Se_3 for annealing at 900 °C under Ar flow. Based on this thermal stability study, the application temperature for the In_3Se_4 under different environment can be determined, in order to preserve its structural integrity.

In summary, *in-situ* synchrotron XRD analysis shows that In_3Se_4 has high thermal stability and remains intact upon heating up to 900 °C in a sealed capillary, which is isolated from ambient O_2. In contrast, In_3Se_4 has a reduced thermal stability of up to 550 °C or 200 °C, when annealed under Ar flow or in an air atmosphere in unsealed systems, respectively. Because of the oxidation of In_3Se_4 induced by O_2 in the heating environment, the annealing at 900 °C under Ar flow (with slight O_2 leaking) or at 400 °C under air can lead to oxidation and decomposition of In_3Se_4 and the formation of In_2O_3 and γ-In_2Se_3. This research demonstrates the influence of heating environment on the thermal stability of In_3Se_4 nanostructures, the products formed under such conditions, and hence the potential applications (or limitations) of this In_3Se_4 phase in high-temperature applications.

This study was supported by the Australian Research Council, the QLD smart state future fellowship (Z.-G.C.); a UQ research foundation excellent award (Z.-G.C.). This work was carried out in part in the Queensland node (the Centre for Microscopy and Microanalysis) of the Australian Microscopy and Microanalysis Research Facility (AMMRF) and on the powder diffraction beamline at the Australian Synchrotron.

[1]T. A. Mary, J. S. O. Evans, T. Vogt, and A. W. Sleight, Science **272**, 90 (1996).
[2]B. L. Pedersen, H. Yin, H. Birkedal, M. Nygren, and B. B. Iversen, Chem. Mater. **22**, 2375 (2010).
[3]H. Yin, B. L. Pedersen, and B. B. Iversen, Eur. J. Inorg. Chem. **2011**, 2733.
[4]T. Dasgupta, C. Stiewe, A. Sesselmann, H. Yin, B. B. Iversen, and E. Mueller, J. Appl. Phys. **113**, 103708 (2013).
[5]Q. Yuan, A. X. Yin, C. Luo, L. D. Sun, Y. W. Zhang, W. T. Duan, H. C. Liu, and C. H. Yan, J. Am. Chem. Soc. **130**, 3465 (2008).
[6]O. A. Baturina, S. R. Aubuchon, and K. J. Wynne, Chem. Mater. **18**, 1498 (2006).
[7]S. Q. Ma, X. S. Wang, D. Q. Yuan, and H. C. Zhou, Angew. Chem. Int. Ed. **47**, 4130 (2008).
[8]Z. Q. Gao, B. X. Mi, G. Z. Xu, Y. Q. Wan, M. L. Gong, K. W. Cheah, and C. H. Chen, Chem. Commun. **2008**, 117.
[9]Y. Inaguma, K. Tanaka, T. Tsuchiya, D. Mori, T. Katsumata, T. Ohba, K. Hiraki, T. Takahashi, and H. Saitoh, J. Am. Chem. Soc. **133**, 16920 (2011).

[10]O. Cambon, G. M. Bhalerao, D. Bourgogne, J. Haines, P. Hermet, D. A. Keen, and M. G. Tucker, J. Am. Chem. Soc. **133**, 8048 (2011).
[11]R. B. Soriano, C. D. Malliakas, J. S. Wu, and M. G. Kanatzidis, J. Am. Chem. Soc. **134**, 3228 (2012).
[12]Z. G. Chen, J. Zou, G. Q. Lu, G. Liu, F. Li, and H. M. Cheng, Appl. Phys. Lett. **90**, 103117 (2007).
[13]D. S. Kong, J. J. Cha, K. J. Lai, H. L. Peng, J. G. Analytis, S. Meister, Y. L. Chen, H. J. Zhang, I. R. Fisher, Z. X. Shen, and Y. Cui, ACS Nano **5**, 4698 (2011).
[14]C. H. Ho, C. H. Lin, Y. P. Wang, Y. C. Chen, S. H. Chen, and Y. S. Huang, ACS Appl. Mater. Interfaces **5**, 2269 (2013).
[15]T. Siciliano, A. Tepore, G. Micocci, A. Genga, M. Siciliano, and E. Filippo, Cryst. Growth Des. **11**, 1924 (2011).
[16]T. Siciliano, M. Tepore, A. Genga, G. Micocci, A. Tepore, and E. Filippo, Mater. Chem. Phys. **136**, 225 (2012).
[17]E. Filippo, M. Siciliano, A. Genga, G. Micocci, A. Tepore, and T. Siciliano, Mater. Res. Bull. **48**, 1741 (2013).
[18]C. H. Liang, G. W. Meng, G. Z. Wang, Y. W. Wang, L. D. Zhang, and S. Y. Zhang, Appl. Phys. Lett. **78**, 3202 (2001).
[19]U. K. Gautam, S. R. C. Vivekchand, A. Govindaraj, and C. N. R. Rao, Chem. Commun. **2005**, 3995.
[20]O. A. Balitskii, N. N. Berchenko, V. P. Savchyn, and J. M. Stakhira, Mater. Chem. Phys. **65**, 130 (2000).
[21]O. A. Balitskii, R. V. Lutsiv, V. P. Savchyn, and J. M. Stakhira, Mater. Sci. Eng., B **56**, 5 (1998).
[22]X. C. Jiang, T. Herricks, and Y. N. Xia, Nano Lett. **2**, 1333 (2002).
[23]P. M. Rao and X. L. Zheng, Nano Lett. **9**, 3001 (2009).
[24]J. Rhyee, K. Lee, S. Lee, E. Cho, S. Kim, E. Lee, Y. Kwon, J. Shim, and G. Kotliar, Nature **459**, 965 (2009).
[25]J. Rhyee, K. Ahn, K. Lee, H. Ji, and J. Shim, Adv. Mater. **23**, 2191 (2011).
[26]X. Shi, J. Y. Cho, J. R. Salvador, J. Yang, and H. Wang, Appl. Phys. Lett. **96**, 162108 (2010).
[27]G. H. Zhu, Y. C. Lan, H. Wang, G. Joshi, Q. Hao, G. Chen, and Z. F. Ren, Phys. Rev. B **83**, 115201 (2011).
[28]Z. G. Chen, G. Han, L. Yang, L. N. Cheng, and J. Zou, Prog. Nat. Sci. **22**, 535 (2012).
[29]J. P. Ye, S. Soeda, Y. Nakamura, and O. Nittono, Jpn. J. Appl. Phys., Part 1 **37**, 4264 (1998).
[30]C. Manolikas, J. Solid State Chem. **74**, 319 (1988).
[31]S. Popovic, A. Tonejc, B. Grzeta-Plenkovic, and R. Trojko, J. Appl. Crystallogr. **12**, 416 (1979).
[32]K. Osamura, Y. Murakami, and Y. Tomiie, J. Phys. Soc. Jpn. **21**, 1848 (1966).
[33]S. Popovic, B. Celustka, and D. Bidjin, Phys. Status Solidi A **6**, 301 (1971).
[34]J. Vanlanduyt, G. Vantendeloo, and S. Amelinckx, Phys. Status Solidi A **30**, 299 (1975).
[35]Y. Li, J. Gao, Q. Li, M. F. Peng, X. H. Sun, Y. Li, G. Yuan, W. Wen, and M. Meyyappan, J. Mater. Chem. **21**, 6944 (2011).
[36]X. Tao and Yi Gu, Nano Lett. **13**, 3501 (2013).
[37]G. Han, Z. G. Chen, C. Sun, L. Yang, L. Cheng, Z. F. Li, W. Lu, Z. M. Gibbs, J. Snyder, K. Jack, J. Drennan, and J. Zou, Cryst. Eng. Comm. **16**, 393 (2014).
[38]G. Han, Z. G. Chen, L. Yang, L. Cheng, J. Drennan, and J. Zou, Cryst. Growth Des. **13**, 5092 (2013).
[39]SpringerMaterials, The Landolt-Börnstein Database, 2013.
[40]O. A. Balitskii, Mater. Lett. **60**, 594 (2006).
[41]A. P. Bakhtinov, Z. D. Kovalyuk, O. N. Sydor, V. N. Katerinchuk, and O. S. Lytvyn, Phys. Solid State **49**, 1572 (2007).